Electronic Supplementary Material (ESI) for ChemComm.

Supporting Information

for

Synthesis, Stability and Reactivity of the First Mononuclear Nonheme Oxoiron(IV) Species with Monoamido Ligation: A Putative Reactive Species Generated from Iron-Bleomycin

Yutaka Hitomi,* Kengo Arakawa and Masahito Kodera

yhitomi@mail.doshisha.ac.jp

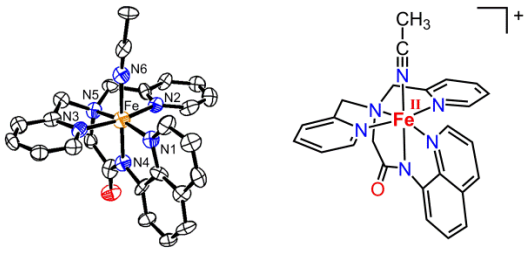

Fig. S1 Crystal structure of $[Fe^{II}(dpaq)(MeCN)]^+$ shown in 50% ellipsoids. The hydrogen atoms were omitted for clarity. Selected bond lengths (Å): Fe–N1, 1.954(3); Fe–N2, 1.95275(3); Fe–N3, 1.934 (3); Fe–N4, 1.905(3); Fe–N5, 1.974(3); Fe–N6, 1.918(3).

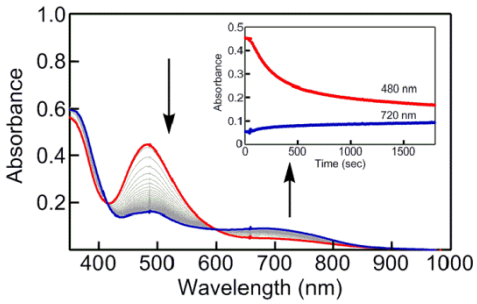

Fig. S2 UV-vis spectral changes observed during the reaction of $[Fe^{II}(dpaq)(MeCN)]^+$ (0.60×10^{-4} M) with O_2 in $MeCN/CH_2Cl_2$ (1:1) at 25 °C. The inset shows the time courses of reaction monitored at 480 nm (red) and 720 nm (blue) due to the formation of $[Fe^{IV}(O)(dpaq)]^+$.

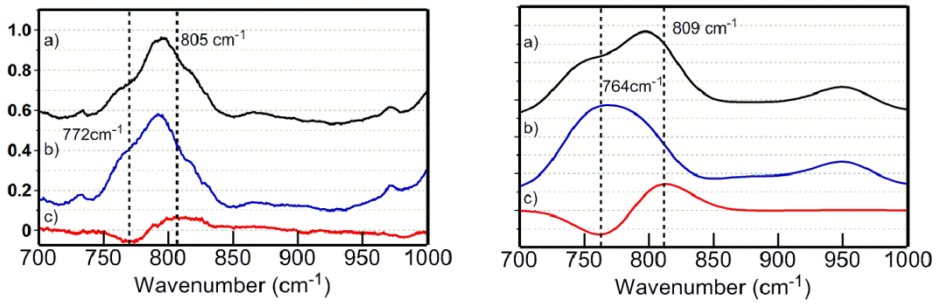

Fig. S3 Experimental (left) and theoretically calculated (right) infrared spectra of $[Fe^{IV}(O)(dpaq)]^+$ prepared using (a) $^{16}O_2$ and (b) $^{18}O_2$ and (c) the differential spectrum.

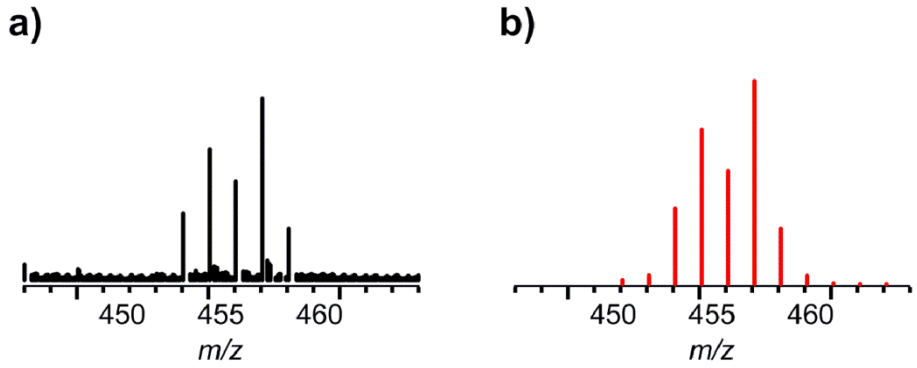

Fig. S4 ESI-MS spectrum (a) of the reaction mixture of $[Fe^{IV}(^{16}O)(dpaq)]^+$ with 100 equiv. of $H_2{}^{18}O$ in $MeCN/CH_2Cl_2$ (1:1). The isotope pattern shown in panel a is assignable to a mixture of four species; $[Fe^{IV}(^{16}O)(dpaq)]^+$, $[Fe^{IV}(^{18}O)(dpaq)]^+$, $[Fe^{III}(dpaq)(^{16}OH)]^+$, and $[Fe^{III}(dpaq)(^{18}OH)]^+$ (15.7 : 27.8 : 16.2 : 40.3), whose simulated spectrum is shown in panel b.

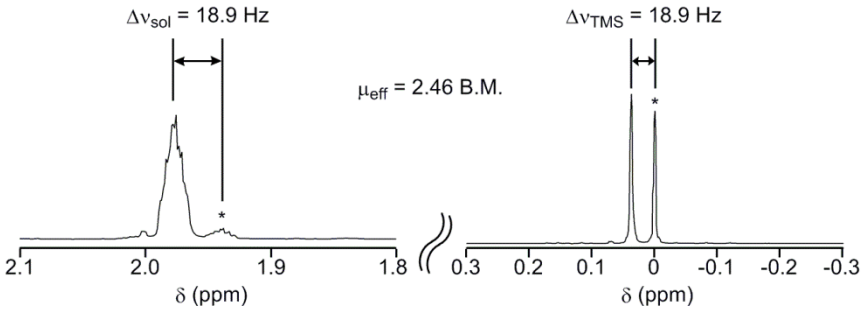

Fig. S5 ^{1}H NMR spectrum of $[Fe^{IV}(O)(dpaq)]^+$ (4.6×10^{-3} M) in CD_3CN at 298 K. The effective magnetic moment was calculated by the modified Evans method. The effective magnetic moment was calculated by the modified Evans method using the following equations: [S1,S2]

$$\mu_{meas} = 0.0618(\Delta\nu T/2fM)^{1/2} = 0.618 \times [(18.9 \times 298)/2 \times 500 \times 4.6 \times 10^{-3}]^{1/2}$$
$$= 2.16$$
$$\chi_{meas} = {\mu_{meas}}^2/(3k_B/N_A\beta^2)T = {\mu_{meas}}^2/8T = 2.16^2/(8 \times 298) = 1.96 \times 10^{-3}$$
$$\chi_D \approx -(MW/2)10^{-6} = -(698.79/2)10^{-6} = -4.22 \times 10^{-4}$$
$$\chi_P = \chi_{meas} - \chi_D = 1.96 \times 10^{-3} - (-4.22 \times 10^{-4}) = 2.54 \times 10^{-3}$$
$$\mu_{eff} = [(3k_B/N_A\beta^2)(\chi_P T)]^{1/2} = (8 \times 2.54 \times 10^{-3} \times 298)^{1/2} = 2.46\ B.M.$$
$$N = -1 + \left(1 + {\mu_{eff}}^2\right)^{1/2} = -1 + (1 + 2.46^2)^{1/2} = 1.65$$

, where μ_{meas} is the measured magnetic moment, $\Delta\nu$ is the difference in frequency (Hz) between the two signals, T is the absolute temperature, f is the NMR oscillator frequency (MHz), M is the molar concentration of the metal complex, χ_{meas} is the measured magnetic susceptibility, k_B is the Boltzmann constant, N_A is Avogadro's number, β is Bohr magneton, χ_D is the diamagnetic magnetic susceptibility, MW is the molecular weight of the sample, χ_P is the paramagnetic magnetic susceptibility, μ_{eff} is the effective magnetic moment, and N is the number of unpaired electrons.

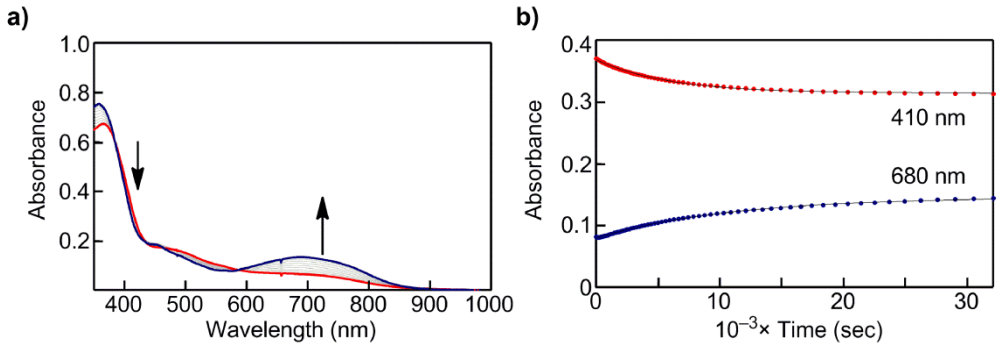

Fig. S6 (a) UV-vis spectral changes of $[Fe^{IV}(O)(dpaq)]^+$ (1.25×10^{-4} M) in MeCN/CH_2Cl_2 (1:1) at 25 °C. (b) The time courses monitored at 410 and 680 nm.

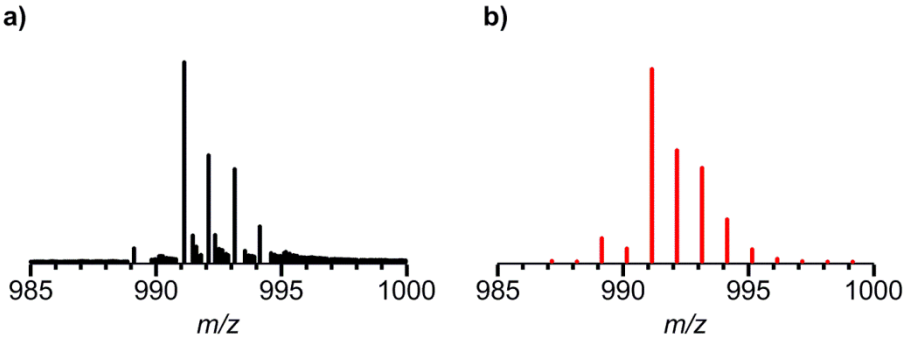

Fig. S7 ESI-MS spectrum (a) of the reaction mixture of $[Fe^{IV}(O)(dpaq)]^+$ (1.25×10^{-4} M) with 800 equiv. of ethylbenzene. The isotope pattern shown in panel a is assignable to $\{[Fe^{III}_2(\mu\text{-}O)(dpaq)_2]ClO_4\}^+$, whose simulated spectrum is shown in panel b.

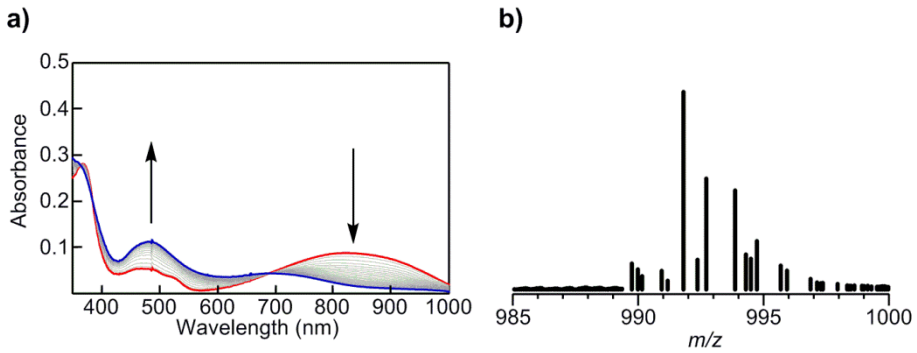

Fig. S8 (a) UV-vis spectral changes in the reaction of $[Fe^{III}(dpaq)(MeCN)]^+$ (0.60×10^{-4} M) with 3 equiv. of NaOH aq. in MeCN at 25 °C. (b) ESI-MS spectra of a reaction mixture of $[Fe^{III}(dpaq)(MeCN)]^+$ (0.60×10^{-4} M) and 3 equiv. of NaOH aq. in MeCN.

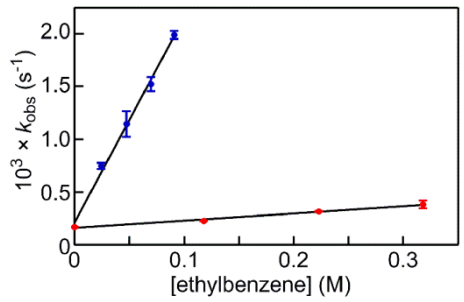

Fig. S9 Plot of k_{obs} vs [ethylbenzene]. Blue and red dots show the data points for ethylbenzene and ethylbenzene-d_{10}, respectively.

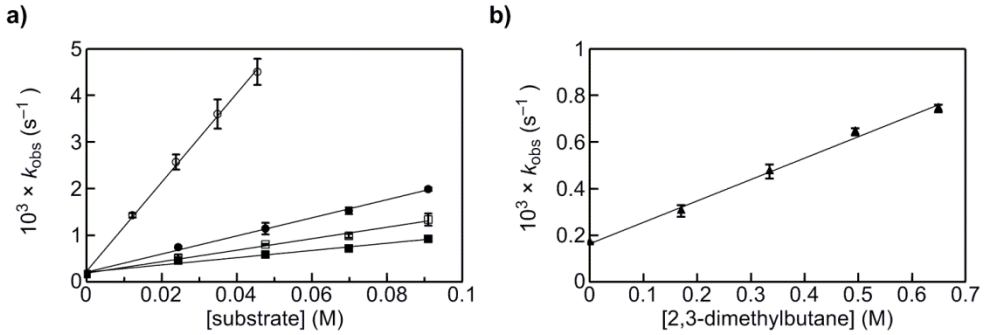

Fig. S10 (a) Plots of k_{obs} vs the concentrations of triphenylmethane (○), cumene (□), ethylbenzene (●) and toluene (■). (b) Plot of k_{obs} vs [2,3-dimethylbutane].

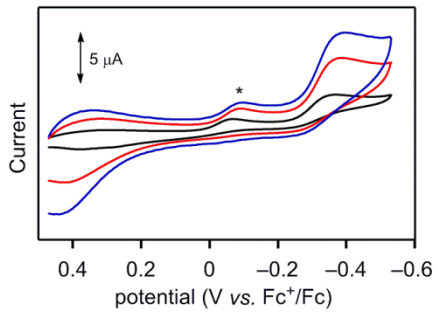

Fig. S11 Cyclic voltammograms of $[Fe^{IV}(O)(dpaq)]^+$ (1.0×10^{-3} M) in deaerated MeCN containing TBAP (0.10 M) with an Au working electrode at 298 K. Scan rate: 10 mV s^{-1} (black), 50 mV s^{-1} (red), 100 mV s^{-1} (blue). Peaks marked with asterisk are the cathodic peak of $[Fe^{III}(dpaq)(OH)]^+$.

Table S1 Summary of the X-ray Crystallographic Data of Fe^{II}(dpaq) Complex.

Compound	$[Fe^{II}(dpaq)(MeCN)](ClO_4)_2 \cdot Et_3NH \cdot MeCN$
Formula	$C_{33}\ H_{41}\ Cl_2\ Fe\ N_8\ O_9$
formula weight	820.49
crystal system	Monoclinic
space group	P 21/c
a, Å	12.1581(2)
b, Å	23.2662(3)
c, Å	13.2420(5)
α, deg	90.00
β, deg	100.4240(10)°
γ, deg	90.00
V, $Å^3$	2789.7(2)
Z	4
F(000)	1400
D_{calcd}, g/cm^{-3}	1.479
T, K	123(2)
crystal size, mm	0.10 0.10 0.10
μ(MoKα), cm^{-1}	0.71073
$2\theta_{max}$, deg	25.35
no. of reflns measd	21288
no. of reflns obsd	6520 >2sigma(I)
no. of variables	387
R^a	0.0721
$R_w{}^b$	0.1542
GOF	0.853

$^aR = \Sigma\ ||F_o| - |F_c|| / \Sigma\ |F_o|$. $^bR_w = [\ \Sigma\ w\ (|F_o| - |F_c|)^2 / \Sigma\ w\ F_o{}^2]^{1/2}$

Table S2 Selected Bond Lengths (Å) and Angles (deg) for Fe^{II}(dpaq) Complex.

Fe(1)-N(1)	1.954(3)
Fe(1)-N(2)	1.952(3)
Fe(1)-N(3)	1.934(3)
Fe(1)-N(4)	1.905(3)
Fe(1)-N(5)	1.974(3)
Fe(1)-N(6)	1.918(3)
C(20)-O(1)	1.227(6)
N(1)-Fe(1)-N(2)	96.45(19)
N(1)-Fe(1)-N(3)	96.76(18)
N(1)-Fe(1)-N(4)	82.8(2)
N(1)-Fe(1)-N(5)	167.33(19)
N(1)-Fe(1)-N(6)	96.1(2)
N(2)-Fe(1)-N(3)	166.7(2)
N(2)-Fe(1)-N(4)	92.34(18)
N(2)-Fe(1)-N(5)	83.28(19)
N(2)-Fe(1)-N(6)	86.58(18)
N(3)-Fe(1)-N(4)	90.67(18)
N(3)-Fe(1)-N(5)	84.13(18)
N(3)-Fe(1)-N(6)	90.66(19)
N(4)-Fe(1)-N(5)	84.5(2)
N(4)-Fe(1)-N(6)	178.37(19)
N(5)-Fe(1)-N(6)	96.6(2)

Table S3 Summary of data for the reactions of $[Fe^{IV}(O)(dpaq)]^+$ with various hydrocarbons.

substrates	BDE_{C-H} (kcal/mol)	k_2 ($M^{-1}s^{-1}$)	product (yield %)
triphenylmethane (1)	81	0.048	triphenylmethanol (48)
cumene (1)	84.5	0.0062	cumyl alcohol (48)
ethylbenzene (2)	87	0.0097	1-phenylenthanol (19)
			acetophenone (9.0)
ethylbenzene-d_{10}		0.00030	
		(KIE = 32)	
toluene (3)	90	0.0039	benzyl alcohol (7)
			benzaldehyde (17)
2,3-dimethylbutane (2)	96.5	0.00046	2-hydroxyl-2,3-dimethylbutane (37)
self-decay			
in MeCN/CH_2Cl_2 (1:1)	98.6 for CH_2Cl_2	0.00016 (s^{-1})	
in MeCN		0.000033 (s^{-1})	

Experimental Procedure

General. All chemicals used in this study were commercial products of the highest available purity and were further purified by the standard methods. The ligand H-dpaq was prepared according to the reported procedure.[S3] Isopropyl 2-iodoxybenzoate was synthesized according to literature procedures and all data were in agreement with published ones.[S4] FT-IR spectra were recorded on a Shimadzu IRAffinity-1 spectrometer equipped with a MIRacle 10 single reflection ATR accessory, and UV-visible spectra were taken on an Agilent 8543 UV-visible spectroscopy system equipped with a Unisoku thermostated cell holder designed for low temperature measurements (USP-203). ^{1}H-NMR spectra were recorded on a JEOL JMN-ECA 500 spectrometer. ESI-MS (electrospray ionization mass spectra) measurements were performed on a JEOL JMS-T100CS spectrometer. Elemental analyses were recorded with a Perkin-Elmer Elemental Analyzer 2400 II. The GC-MS analysis was performed with a Shimadzu GC-MS-QP5000 gas chromatography equipped with a Shimadzu CBP1 capillary column (25 m × 0.32 mm).

Synthesis of Iron Complexes

Caution: *Perchlorate salts of metal complexes are potentially explosive and should be handled in small quantities with care.*

Synthesis of Fe^{II}(dpaq) Complex

$Fe(ClO_4)_2{\cdot}6H_2O$ (0.57 g, 1.6 mmol) was placed in a glass vial, and MeCN (5.0 mL) was added to form a yellow solution. This solution was then added to a second vial containing H-dpaq[S3] (0.50 g, 1.3 mmol) in MeCN (15 mL). To the mixture was added triethylamine (0.25 mL, 2.0 mmol). The mixture turned to red. 3 h later the reaction mixture was added excess diethylether. The resulting red crystals were collected, and after vacuum-drying a red crystalline material was isolated weighing 0.383 g (47%). FT-IR (ATR, cm^{-1}) 1600 (C=O), 1093 and 621 (ClO_4^-); Anal. Calcd for $[Fe(dpaq)(MeCN)]ClO_4{\cdot}0.5CH_2Cl_2$ ($C_{25.5}H_{24}Cl_2FeN_6O_5$): C, 49.30; H, 3.89; N, 13.53. Found: C, 49.45; H, 3.80; N, 13.08. UV-vis (MeCN): 480 nm (7385 M^{-1} cm^{-1}), 350 nm (6576 M^{-1} cm^{-1}). ESI-MS, positive mode: *m*/*z* 438.08 $[Fe^{II}(dpaq)]^+$.

X-ray Structure Determination:

The single crystal suitable for X-ray analysis was obtained according to the above procedure. Crystal, data collection, and refinement parameters are given in Tables S1 and S2. A suitable crystal for single-crystal X-ray diffraction was selected and mounted on a RIGAKU R-Axis Rapid diffractometer with graphite-monochromated Mo K_α radiation (λ = 0.71075 Å).

Synthesis of $Fe^{IV}(O)(dpaq)$ Complex

Method I: To a 0.125 mM solution of $[Fe^{II}(dpaq)(MeCN)]ClO_4$ in $MeCN/CH_2Cl_2$ (1/1) was added 0.5 equivalents of isopropyl 2-iodoxybenzoate (50 µL) at −40°C. The characteristic band of $[Fe^{IV}(O)(dpaq)]^+$ at 720 nm reached a maximum after 30 min.

Method II: $[Fe^{II}(dpaq)(MeCN)]ClO_4$ (2.45 mg, 4.25 µmol) was dissolved in 85 mL of $MeCN/CH_2Cl_2$ (1/1) and allowed to stir until the reaction mixture became homogeneous. The resulting red solution was treated with O_2 causing a color change to brown. The solvent was removed in vacuo at −20°C to afford 2 mg (92 %) of the solid product. FTIR (ATR, cm^{-1}) ν(C=O) 1604, $\nu(Fe=^{16}O)$ 804, $\nu(Fe=^{18}O)$ 777; Anal. Calcd for $[Fe^{IV}(O)(dpaq)]ClO_4 \cdot 0.5CH_2Cl_2$ ($C_{23.5}H_{21}Cl_2FeN_6O_5$): C, 47.34; H, 3.55; N, 11.75. Found: C, 47.53; H, 3.82; N, 11.85. UV-vis (MeCN): 686 nm (713.5 M^{-1} cm^{-1}), 912 nm (113.6 M^{-1} cm^{-1}). ESI-MS, positive mode: *m*/*z* 454.04 $[Fe^{IV}(dpaq)(O)]^+$, 456.04 $[Fe^{IV}(dpaq)(^{18}O)]^+$.

NMR Measurements for Spin State Determination: ^{1}H NMR spectra were measured with a JEOL JMN-ECA500 (500 MHz) NMR spectrometer. The spin state of $[Fe^{IV}(O)(dpaq)]^{+}$ was determined using the modified ^{1}H NMR method of Evans at 298 K. A 25μL Drumond microdispenser replacement tube (sealed capillary) containing 80 μL of CD_3CN (with 1.0% TMS) was inserted into a normal NMR tube containing $[Fe^{IV}(O)(dpaq)]^{+}$ (600 μL, 4.6×10^{-3} M) dissolved in CD_3CN (with 1.0% TMS).

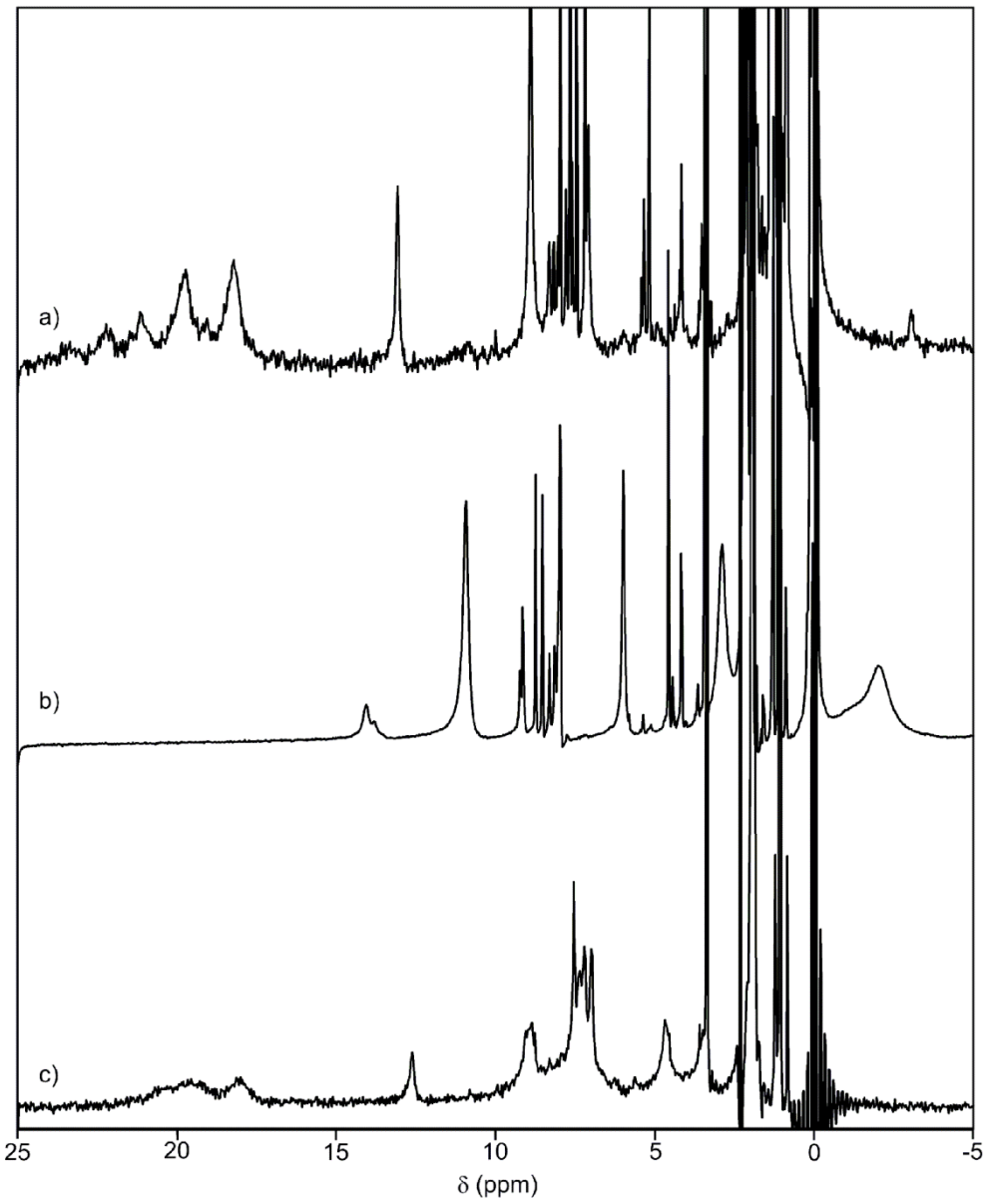

Fig. S12 ^{1}H NMR spectrum (500 MHz) of $[Fe^{IV}(O)(dpaq)]^{+}$ generated by the reaction of $[Fe^{II}(dpaq)(MeCN)]^{+}$ (4.6×10^{-3} M) with 0.5 equiv. of isopropyl 2-iodoxybenzoate (a), $[Fe^{III}(dpaq)(MeCN)]^{2+}$ (b), and $[Fe^{II}(dpaq)(MeCN)]^{+}$ (c) in CD_3CN at 298 K.

Reactivity Studies:

A solution of $[Fe^{IV}(O)(dpaq)]^+$ (0.125 mM) in MeCN/CH_2Cl_2 (1/1) was prepared by the reaction of $[Fe^{II}(dpaq)(MeCN)]^+$ with 0.5 equiv. of isopropyl 2-iodoxybenzoate. Substrates were added to the stirred solutions under Ar. The decay of $[Fe^{IV}(O)(dpaq)]^+$ was monitored on an Agilent 8543 UV-visible spectroscopy system at 25°C. The solutions at the end of the reaction were then analyzed by GC/MS (with nitrobenzene as a quantification standard). The data obtained from these studies are collected in Table S3. The k_1 value was calculated by using the following equations:

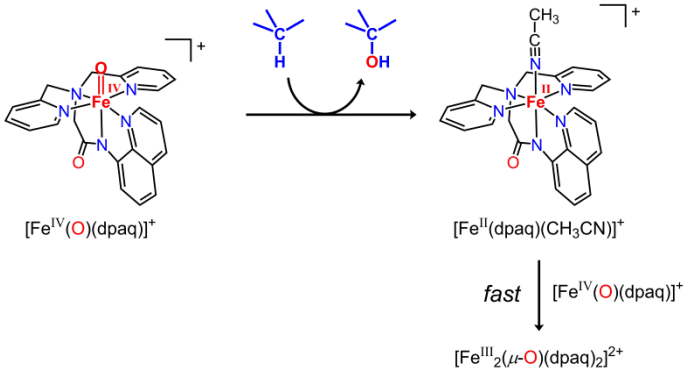

$$\mathrm{A} + \mathrm{B(excess)} \xrightarrow{k_2} \mathrm{C}$$
$$\mathrm{C} + \mathrm{A} \xrightarrow{k_2'} \mathrm{D}$$

$$\frac{d[\mathrm{C}]}{dt} = k_2[\mathrm{A}][\mathrm{B}] - k_2'[\mathrm{C}][\mathrm{A}] = 0 \quad \Leftrightarrow \quad k_2[\mathrm{B}] = k_2'[\mathrm{C}]$$

$$\frac{d[\mathrm{A}]}{dt} = -k_2[\mathrm{A}][\mathrm{B}] - k_2'[\mathrm{C}][\mathrm{A}] = -2k_2[\mathrm{A}][\mathrm{B}]$$

$$\therefore k_{obs} = 2k_2[\mathrm{B}]$$

, where A is the concentration of $[Fe^{IV}(O)(dpaq)]^+$, B is the concentration of substrate, C is the concentration of $[Fe^{II}(dpaq)]^+$, D is the concentration of $[Fe^{III}{}_2(\mu\text{-}O)(dpaq)_2]^{2+}$.

Electrochemical Measurements: Cyclic voltammetric measurements were performed on a BAS CV-50W electrochemical analyzer in deaerated MeCN containing 0.1 M *n*-Bu_4NClO_4 as a supporting electrolyte and 1 mM $[Fe^{IV}(O)(dpaq)]^+$. The Au working electrode (BAS) was polished with BAS polishing alumina suspension and rinsed with MeCN before use. The counter electrode was a platinum wire. All potentials were reported with respect to the ferrocene/ferrocenium redox couple (Fc/Fc^+).

Density Functional Calculations:

The structure of $S = 1$ $[Fe^{IV}(O)(dpaq)]^+$ was fully optimized using the BP method in combination with TZV(2pf) basis sets on Fe, TZV(2d) basis sets on C, N, and O, and TZP(p) basis sets on H. The vibrational frequencies of the fully optimized complex were again calculated with BP/TZVP, showing no imaginary frequencies. All of these calculations were performed using the program ORCA version 2.8.[S5]

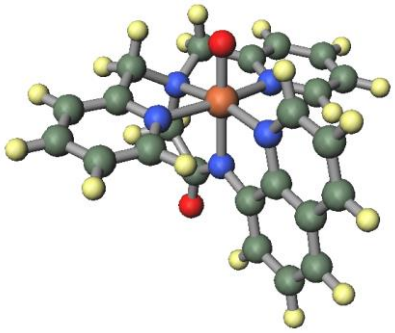

Fig. S13 Fully optimized structures of $[Fe^{IV}(O)(dpaq)]^+$ for $S = 1$, obtained with BP/TZVP. Structural data are given in Table S4.

Table S4. Coordinates [Å] of $S = 1$ $[Fe^{IV}(O)(dpaq)]^+$ fully optimized.

Atom	Coordinates		
	x	y	z
Fe	-0.61206	0.073779	0.528363
H	0.495741	-0.92236	3.170272
C	1.327656	-1.02772	2.472463
N	1.082062	-0.64348	1.214637
C	3.599282	-1.64344	1.918878
C	2.073349	-0.73929	0.259324
C	2.585994	-1.53531	2.854772
C	3.370956	-1.24363	0.575876

C	1.731539	-0.30934	-1.06064
H	2.738871	-1.83727	3.890672
H	5.330298	-1.69292	-0.25057
H	4.578059	-2.03531	2.202369
C	2.707638	-0.38939	-2.05698
H	2.464975	-0.06416	-3.0667
C	3.991897	-0.88935	-1.74211
H	4.735793	-0.94238	-2.53905
C	4.332136	-1.30981	-0.46678
C	-0.1854	0.614195	-2.27452
O	0.282965	0.73981	-3.40569
N	0.422129	0.141982	-1.15162
N	-2.11719	0.82885	-0.58191
C	-1.65111	1.023657	-2.00789
H	-1.7625	2.080974	-2.28736
H	-2.29339	0.443065	-2.68434
C	-3.21316	-0.18242	-0.47512
H	-3.99689	-0.0097	-1.22961
H	-3.65371	-0.07642	0.528071
C	-2.46727	2.121601	0.083652
H	-3.01813	1.871945	1.003218
H	-3.10731	2.746194	-0.55936
N	-0.17155	2.009869	0.815282
C	0.122144	4.770969	1.010198
C	0.987071	2.541772	1.247719
C	-1.19891	2.831954	0.476471
C	-1.07818	4.218324	0.556177
C	1.168077	3.918558	1.365058
H	1.777358	1.838399	1.503658
H	-1.91566	4.853941	0.266473
H	2.12102	4.307133	1.723037
H	0.238313	5.853198	1.082587
O	-1.48012	0.01047	1.968532
N	-1.36991	-1.68547	-0.07101
C	-2.69642	-3.91815	-1.07324
C	-0.77702	-2.89397	-0.05231

C	-2.62314	-1.564	-0.58132
C	-3.30808	-2.66237	-1.0977
C	-1.41312	-4.03467	-0.53845
H	0.227154	-2.93429	0.364758
H	-4.30878	-2.53284	-1.5105
H	-0.89855	-4.99452	-0.50084
H	-3.21487	-4.79187	-1.46927

References

S1. G. A. Bain, J. F. Berry, *J. Chem. Educ.*, 2008, **85**, 532.

S2. D. F. Evans, D. A Jakubovic, *J. Chem. Soc., Dalton Trans.*, 1988, 2927.

S3. Y. Hitomi, K Arakawa, T Funabiki, M Kodera, *Angew. Chem., Int. Ed.*, 2012, **51**, 3448.

S4. V. V. Zhdankin, A. Y. Koposov, D. N. Litvinov, M. J. Ferguson, R. McDonald, T. Luu, R. R. Tykwinski, *J. Org. Chem.*, 2005, **70**, 6484.

S5. F. Neese, ORCA—An ab Initio, Density Functional, and Semiempirical Program Package (Universität Bonn, Bonn, Germany) Version 2.8, 2010.